View metadata, citation and similar papers at core.ac.uk

brought to you by CORE

provided by Cronfa at Swansea University

Cronfa - Swansea University Open Access Repository

This is an author produced version of a paper published in:
Physics of Metals and Metallography

Cronfa URL for this paper:
http://cronfa.swan.ac.uk/Record/cronfa37646

Paper:
Riva, S., Lavery, N., Yusenko, K. & Brown, S. (2018). Scandium-based hexagonally-closed packed multi-component alloys. *Physics of Metals and Metallography*(8)

This item is brought to you by Swansea University. Any person downloading material is agreeing to abide by the terms of the repository licence. Copies of full text items may be used or reproduced in any format or medium, without prior permission for personal research or study, educational or non-commercial purposes only. The copyright for any work remains with the original author unless otherwise specified. The full-text must not be sold in any format or medium without the formal permission of the copyright holder.

Permission for multiple reproductions should be obtained from the original author.

Authors are personally responsible for adhering to copyright and publisher restrictions when uploading content to the repository.

http://www.swansea.ac.uk/library/researchsupport/ris-support/

НАЗВАНИЕ РАЗДЕЛА

УДК

Scandium-based hexagonally-closed packed multi-component alloys

Sephira Riva, Stephen G.R. Brown, Nicholas P. Lavery, and Kirill V. Yusenko
College of Engineering, Swansea University, Bay Campus, Swansea SA1 8QQ, Wales, UK
e-mail: k.yusenko@swansea.ac.uk

Since their early development, High-Entropy Alloys have fueled the investigation of exotic metal combinations. Here, we present a strategy for rational design of a library for multi-component alloys based on six *hcp*-structured metals. Seven five- and six-component equimolar alloys based on Co, Gd, Y, Sc, Ti and Zr were prepared via induction melting and characterized by PXRD, SEM –EDX and Vicker's hardness. They all present ternary hexagonal phases (ScTiZr or GdScY) co-existing with one or more cubic phases and intermetallic compounds. Both ScTiZr and GdScY appear promising as the starting point for new single-phase High-Entropy Alloys families.

Keywords: High-entropy alloys; Hexagonal close-packed alloys; Scandium.

INTRODUCTION

High-Entropy Alloys (HEAs) are often defined as multi-principal component alloys containing more than 5 elements in 5-35 at.%. While this composition-based definition gives no indication on the structure or scope of the alloy, the search for HEAs coincides in most cases with the search for multicomponent single-phase solid solutions [1, 2]. Over 99 % of reported HEA consist of cubic (*bcc* or *fcc*) single or duplet co-existing phases. On the other hand, *hcp*-structured HEAs are still an unexplored field. This is partly because previous research has tackled only a small portion of the composition space, focusing mostly on some transition or refractory metals [3].

The preparation of *hcp*-structured HEAs has been mostly driven by uncommon elements, especially those belonging to the lanthanides series. $Dy_{20}Gd_{20}Lu_{20}Tb_{20}Y_{20}$ and $Dy_{20}Gb_{20}Lu_{20}Tb_{20}Tm_{20}$ HEA consist of an *hcp* alloy plus an unknown phase [4]. Two-phase *hcp* structures were reported in the six-component $Hf_{20}La_{20}Sc_{20}Ti_{20}Y_{20}Zr_{20}$ alloy [5]; one of these was isolated as the equiatomic $Hf_{25}Sc_{25}Ti_{25}Zr_{25}$ [6]. Exceptions are the $Co_{25}Fe_{25}Ni_{25}Ti_{25}$ alloy [7], which is a mixture of *hcp* and *fcc* phases, and the predicted $Co_{25}Os_{25}Re_{25}Ru_{25}$ alloy [2].

So far, the only single phase *hcp* HEAs are $AlLi_{0.5}MgScTi_{1.5}$, produced via mechanical milling followed by high temperature annealing [8], and $Dy_{20}Gd_{20}Ho_{20}Tb_{20}Y_{20}$, synthesized via arc melting from pure metals [9]. Phase pure three- and four-component alloys have also been reported (MoRhRu and MoPdRhRu); but, using the composition definition, strictly speaking they cannot be considered as HEAs [10].

The idea of combining *hcp*-structured elements to investigate the formation of *hcp* alloys in multi-principal component alloys may seem *naïve*, but the State of the Art of *hcp* HEA highlights that even *pan*-hexagonal metallic compositions usually form poly-phase mixtures of *hcp*-alloys or intermetallic compounds. Furthermore, as in the case of $AlLi_{0.5}MgScTi_{1.5}$, melting temperatures of individual metals are sometimes so different that mechanical alloying substitutes more traditional synthesis routes.
The aim of this study was to prepare a combinatorial library of multi-principal component alloys containing only high-temperature melting *hcp*-structured metals through induction melting and then identify hexagonally-structured single-phase solid solutions. The chosen metals, combined in equal atomic concentrations, were Co, Gd, Sc, Ti, Y and Zr.

EXPERIMENTAL

The target alloys were prepared using induction melting. Co, Ti and Zr were taken as powders or rods, while Gd, Sc and Y as pieces. All metals were purchased from Goodfellows at ≥ 99% purity, mixed, placed in a BN crucible (Kennametal) and melted using an induction coil in a glove-box operated under Ar pressure (scrubbed by catalysts to O_2 levels below 500 ppm) to protect metals from high-temperature oxidation. In all cases, complete melting was achieved above 1600 °C. After 5 minutes at the melting temperature the samples were cooled down naturally to room temperature (2 minutes). All as-cast materials were annealed in a dynamic vacuum (10^{-2} Pa) at 900 °C for 12 h, followed by 2 hours of natural cooling to room temperature.

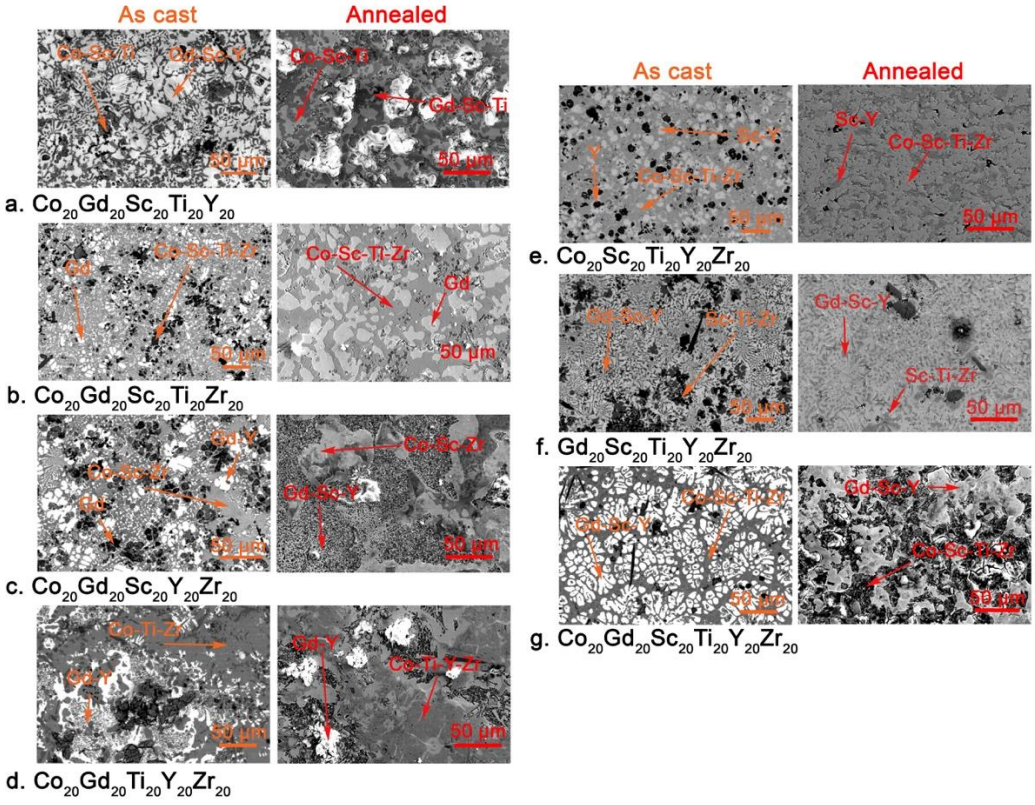

Fig. 1. SEM images of the as-cast (*orange*, *left*) and annealed (*red*, *right*) alloys. Element distributions of different areas as from EDX maps are highlighted.

For characterization, all samples were mounted in carbonized resin, polished using MetaDiTM Supreme Polycrystalline Diamond Suspension (1 µm) and chemically etched with a solution of HNO_3 5 vol.% in ethanol. Morphology and elemental composition were analyzed using a Hitachi S-4800 Field Emission scanning-electron microscope (SEM) equipped with energy dispersive X-ray (EDX) analyzer. The average elemental composition was obtained from 0.5×0.5 mm maps. Vickers hardness was investigated on a WilsonR VH3100 Automatic Knoop/Vickers Hardness tester: 25 individual points under a 9.81 N (1 kg) testing load were measured to get statistically significant results. Powder X-ray diffraction patterns were collected from the powdered samples. Powders were fixed between two Kapton foils and measured at room temperature in transmission mode at the ID06A beam-line at the European Synchrotron Radiation Facility (position sensitive detector, $\lambda = 0.22542$ Å). Phase identification was performed via automated and manual search-match through the using the Inorganic Crystal Structure Database [11].

RESULTS AND DISCUSSION

Seven High-Entropy Alloys containing 5 or 6 *hcp*-structured elements were prepared by induction melting (Table 1). All samples are multiphase (Figure 1) and contain at least one *hcp* phase (Figure 2). Due to the large difference in atomic radius and electronegativity among the elements, only a few of them form solid solutions while several form stable intermetallic compounds [12-14].

To examine temperature-induced effects in melted compositions and equilibrated systems, as-cast and thermally annealed samples (900 °C, 12 hours in dynamic vacuum 10^{-2} Pa) were investigated. All samples appear to be multi-phase both before and after annealing (see Figure 1), with annealing affecting microstructure and mechanical properties of the alloys, but having low impact on element distributions. Elemental distribution maps obtained by EDX analysis suggest the following phases and elemental separation in the samples. For $Co_{20}Gd_{20}Sc_{20}Ti_{20}Y_{20}$ (figure 1a) Co, Sc and Ti segregate from Gd and Y. $Co_{20}Gd_{20}Sc_{20}Ti_{20}Zr_{20}$ (figure 1b) displays a Co—Ti—Zr matrix and Gd-rich areas; scandium is homogeneously distributed. In $Co_{20}Gd_{20}Sc_{20}Y_{20}Zr_{20}$ (figure 1c), Co—Sc—Zr regions segregate from the matrix, surrounded by Gd and Y.

Table 1. Parameters of elements adopting *hcp*-structure used to produce the HEA library [14].

Element	Atomic number	Atomic radius, Å	Lattice constant, Å		Pauling electronegativity	T_m, °C
			a	*c*		
Cobalt	27	1.25	2.5061	4.0695	1.7	1495
Gadolinium	64	1.79	3.6330	5.7739	1.2	1312
Scandium	21	1.64	3.2899	5.2529	1.3	1539
Titanium	22	1.46	2.9509	4.6826	1.5	1670
Yttrium	39	1.81	3.6474	5.3706	1.2	1526
Zirconium	40	1.60	3.2312	5.1477	1.4	1850

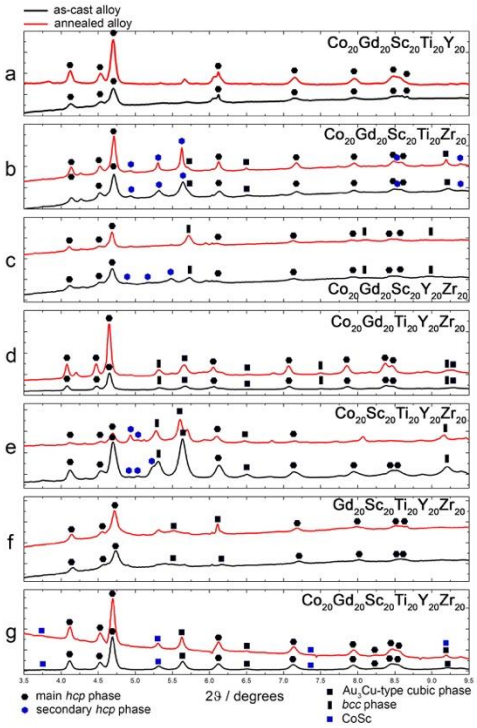

Fig.2 Powder X-Ray Diffraction patterns (λ = 0.22542 Å) of the as-cast (*black*) and annealed (*red*) alloys. Lines corresponding to primary and secondary phases are marked.

For $Co_{20}Gd_{20}Ti_{20}Y_{20}Zr_{20}$ (figure 1d), Y is homogeneously dispersed. After annealing Gd-Y and Co—Ti—Y—Zr areas are formed. In the case of the $Co_{20}Sc_{20}Ti_{20}Y_{20}Zr_{20}$ (figure 1e) alloy, areas rich in Sc, Ti and Zr dissolve during heat treatment, forming a matrix in which Sc—Y-rich structures grow. $Gd_{20}Sc_{20}Ti_{20}Y_{20}Zr_{20}$ (figure 1f) presents a Gd—Y matrix and Sc—Ti—Zr alloy. Finally, the six-elements $Co_{16}Gd_{16}Sc_{16}Ti_{16}Y_{16}Zr_{16}$ (figure 1g) alloy displays two main areas: Co—Sc—Ti—Zr and Gd—Sc—Y.

In the six-component alloy the two phases ScTiZr and GdYSc co-exist and scandium is homogeneously dispersed in the matrix. We can therefore deduce that the formation of a scandium-containing single-phase solid solution is deeply affected by the balance between atomic size and chemical similarity. If the former prevails, scandium mixes preferably with Ti and Zr. If chemical similarity between scandium and rare-earth metals dominates, Sc dissolves in Y and Gd. The formation of the ScTiZr solid solution is consistent to the reported $Hf_{25}Sc_{25}Ti_{25}Zr_{25}$ single-phase *hcp* alloy [6], whereas, to the authors' knowledge, the GdYSc solid solution has never been used as the starting point for the development of a multi-component single-phase system. To do so, computational modelling based on binary and ternary phase diagrams will be an essential requirement [15,16]. Nevertheless, knowledge about *hcp*-metals ternary phase diagrams is still fragmented: the intrinsic complexity of some of these binary phase diagrams, which contain a huge variety of intermetallic compounds, poses a challenge to the exploration of the hyper-dimensional composition space. To the authors knowledge, out of all possible combinations with Co, Gd, Sc, Ti, Y and Zr, only an isothermal section (T =773 K) of the Co-Gd-Ti phase diagram has been investigated [17].

Yttrium disperses in the matrix homogeneously only in the absence of scandium. This is an unexpected result, because yttrium and scandium are often considered chemically interchangeable and because the binary Y-Sc phase diagram displays complete miscibility in both solid and liquid states. This suggests that the addition of Y to ScTiZr would not lead to a single-phase four-component alloy, but rather to the segregation of Sc—Y-rich areas in a ScTiZr matrix.

The PXRD patterns of the as-melted and annealed alloys are very complex and show several crystalline phases (Figure 2 and Table 2). The broad diffraction

Table 2. Phase composition from synchrotron PXRD profiles and Vicker's hardness values (1 HV load) before and after annealing.

Alloy composition	Main phase ($P6_3/mmc$) Cell parameters, Å	Secondary phase(s) cell parameters, Å	Vicker's Hardness, HV	
			As melted	Annealed
$Co_{20}Gd_{20}Sc_{20}Ti_{20}Y_{20}$	a = 3.62(2); c = 5.70(3)	unindexed phase(s)	218(28)[1]	186(29)
$Co_{20}Gd_{20}Sc_{20}Ti_{20}Zr_{20}$	a = 3.61(2); c = 5.71(3)	$P6_3/mmc$ (a = 3.03; c = 4.80) $Pm\bar{3}m$ (a = 3.96)	345(35)	318(145)[2]
$Co_{20}Gd_{20}Sc_{20}Y_{20}Zr_{20}$	a = 3.62(3); c = 5.71(1)	$Im\bar{3}m$ (a = 3.20(1)) $P6_3/mmc$ (a = 3.05(2); c = 5.00(3))	257(15)	233(41)
$Co_{20}Gd_{20}Ti_{20}Y_{20}Zr_{20}$	a = 3.65(7); c = 5.76(4)	$Pm\bar{3}m$ (a = 3.94(5)) $Im\bar{3}m$ (a = 3.44(3))	251(72)	429(85)
$Co_{20}Sc_{20}Ti_{20}Y_{20}Zr_{20}$	a = 3.62(9); c = 5.71(2)	$P6_3/mmc$ (a = 3.02(2); c = 4.90(3)) $Pm\bar{3}m$ (a = 3.97(1)) $Im\bar{3}m$ (a = 3.44(3))	358(23)	825(47)
$Gd_{20}Sc_{20}Ti_{20}Y_{20}Zr_{20}$	a = 3.59(3); c = 5.66(3)	$Pm\bar{3}m$ (a = 4.15(3))	289(22)	174(22)
$Co_{16}Gd_{16}Sc_{16}Ti_{16}Y_{16}Zr_{16}$	a = 3.62(2); c = 5.70(3)	$Pm\bar{3}m$ (a = 3.97) CoSc $Pm\bar{3}m$ (a = 3.435(1))	269(31)[1]	188(38)

[1] load of 0.2 HV; [2] load of 0.3 HV

lines characteristic for *hcp*-structured alloys might mask several phases with close cell parameters [18].

In all cases an *hcp*-structured alloy has been detected as the main phase, with two or more cubic phases (Au_3Cu and *B2* structure types) as minor admixtures. The PXRD profile for $Co_{16}Gd_{16}Sc_{16}Ti_{16}Y_{16}Zr_{16}$ (Figure 2g) also shows lines corresponding to the CoSc intermetallic phase ($Pm\bar{3}m$, a = 3.435). For $Co_{20}Gd_{20}Sc_{20}Y_{20}Zr_{20}$ heat treatment results in the dissolution of the secondary *hcp* phase (probably pure Gd, which goes to enrich the GdYSc phase), which could explain its low decrease in hardness in comparison with other alloys. Other lines in the profiles are too broad to be indexed.

As far as mechanical properties are concerned (Table 2), Vicker's hardness values refer to the alloys overall compositions and microstructures. Such values are lower than those found in the literature for known HEAs, and generally drop after heat treatment. Exceptions are the $Co_{20}Sc_{20}Ti_{20}Y_{20}Zr_{20}$ alloy, which shows remarkably high Vicker's hardness after annealing (825(47) HV), and the $Co_{20}Gd_{20}Ti_{20}Y_{20}Zr_{20}$ alloy, which displays a 50 % hardness enhancement. The increase in hardness might be due to the presence of the same intermetallic, of crystal structure $Im\bar{3}m$ (a = 3.44(3)). All alloys present high brittleness and crack formation under relatively low load.

CONCLUSIONS

The design of a combinatorial library of multi-principal elements alloys from *hcp* metals highlights that the formation of single-phase solid solutions, achievable as an *fcc* or *bcc* phase when only cubic metals are involved, is hindered by the formation of intermetallics in the case of *hcp* metals. The creation of a single-phase *hcp*-structured HEA from *hcp*-structured metals appears to be impossible. Although multicomponent *hcp* alloys are formed, cubic intermetallics as secondary phases are also present.

The possibility of using three-component scandium- or yttrium-containing alloys as the starting point for High-Entropy Alloys is discussed. The formation of the ScTiZr solid solution is consistent with the reported $Hf_{25}Sc_{25}Ti_{25}Zr_{25}$ single-phase *hcp* alloy [6], while the GdYSc solid solution shows the potential to become the basis for the development of a multi-component single-phase *hcp* alloying system. This suggests that phase diagrams are not enough to predict the behaviour of chemically similar metals in complex systems, electronic density and atomic size should also be considered for the design of new multi-principal alloy combinations.

REFERENCES

1. *Yeh J-W.* Overview of High-Entropy Alloys. In: *High-Entropy Alloys: Fundamentals and applications*, 1st ed.; Gao, M.C.; Yeh, J-W.; Liaw, P.K.; Zhang, Y., Eds.; Springer: Cham (ZG), Switzerland, 2016; Volume 1, pp. 1–20.
2. *Gao M.C., Alman D.E.* Searching for next single-phase High-Entropy Alloy Compositions // Entropy 2013. V. 1. P. 4504-4519.
3. *Miracle D.B., Senkov, O.N.* A critical review of high entropy alloys and related concepts // Acta Mat 2017. V. 122. P. 448-511.
4. *Takeuchi A., Amiya K., Wada T., Yubuta K., Zhang W.* High-Entropy Alloys with a hexagonal close-packed structure designed by equi-atomic alloy strategy and binary phase diagrams // JOM 2014. V. 66. P. 1984-1992.
5. *Takeuchi A., Amiya K., Wada T., Yubuta K.* Dual HCP structured formed in senary ScYLaTiZrHf multi-principal-elements alloy // Intermet 2016. V. 69. P. 103-109.
6. *Rogal L., Czerwinski F., Jochym P.T., Litynska-Dobrzynska L.* Microstructure and mechanical properties of the novel Hf25Sc25Ti25Zr25 equiatomic alloy with hexagonal solid solutions // Mat Design 2016. V. 92. P. 8-17.
7. *Tsau C-H.* Phase transformation and mechanical behaviour of TiFeCoNi alloy during annealing // Mat Sci Eng A 2009. V. 501. P. 81-86.
8. *Youssef K.M., Zaddach A.J., Niu C., Irving D.L.; Koch C.C.* A novel low density, high hardness, high-entropy alloy with close-packed single-phase nanocrystalline structures // Mat Res Lett 2014. V. 3. P. 95-99.
9. *Feuerbacher M., Heidelmann M., Thomas C.* Hexagonal High-Entropy Alloys // Mat Res Lett 2015. V. 3. P. 1-6.
10. *Paschoal J.O.A., Kleykamp H., Thummler F.* Phase equilibria in the quaternary molybdenum-ruthenium-rhodium-palladium system // Z. Metallkd 1983. V. 74, P. 652.
11. *Hellenbrandt M.* The inorganic crystal structure database (ICSD) – present and future // Chr Rev 2004. V. 10. P. 17-22.
12. *Riva S., Yusenko K.V., Lavery N.P., Jarvis D.J., Brown S.G.R.* The scandium effect in multicomponent alloys // Int Mat Rev 2016. V. 61. P. 1-26.
13. *Riva S., Fung C.M., Searle J.R., Clark R.N., Lavery N.P., Brown S.G.R., Yusenko K.V.* Formation and disruption of W-phase in High-Entropy Alloys // Metals 2016. V. 6. P. 1-8.
14. *Samsonov G.V.* Handbook of the physicochemical properties of the elements, 1st ed.; IFI/Plenum: New York-Washington, USA, 1968; pp. 248.
15. *Toda-Caraballo I., Rivera-Dìaz—del-Castillo P.E.J.* Modelling and design of magnesium and high-entropy alloys through combining statistical and physical models // JOM 2015. V. 67. P. 108-117.
16. *Toda-Caraballo I., Rivera-Dìaz—del-Castillo P.E.J.* Modelling solid solution hardening in high-entropy alloys // Acta Mat. 2015. V. 85. P. 14-23.
17. *Mattern N., Zinkevich M., Han J.H., Löser W.* Experimental and thermodynamic assessment of the Co-Gd-Ti system // CALPHAD: Computer Coupling of Phase Diagrams and Thermochemistry 2016. V. 54. P. 144-157.
18. *Dahlborg U., Cornide J, Calvo-Dahlborg M., Hansen T.C., Fitch A., Leong Z., Chambreland S, Goodall R.* Structure of some CoCrFeNi and CoCrFeNiPd multicomponent HEA alloys by diffraction techniques // J All Compd 2016. V. 681. P. 330-341.

ACKNOWLEDGEMENTS

The Authors gratefully acknowledge the financial support provided by the Welsh Government and Higher Education Funding Council for Wales through the Sêr Cymru National Research Network in Advanced Engineering and Materials and by the European Space Agency (contract number 4000111643/NL/PA). KVY is grateful to the EPSRC Impact Acceleration Account for financial support. The authors thank the Materials Advanced Characterisation Centre (MACH1) at Swansea University and the European Synchrotron Radiation Facility (Grenoble, France) for providing measurement time and technical support.